ISSN 1070-3284, Russian Journal of Coordination Chemistry, 2022, Vol. 48, No. 6, pp. 353–361. © The Author(s), 2022. This article is an open access publication.
Russian Text © The Author(s), 2022, published in Koordinatsionnaya Khimiya, 2022, Vol. 48, No. 6, pp. 343–351.

Cyclometallated Ruthenium Complex with 3,3',5,5'-Tetramethyl-1,1'-biphenyl-4,4'-bipyrazole and 2,2'-Dicarboxybipyridine: Synthesis, Optical Properties, and Quantum Chemical Modeling

M. A. Lavrova[a, *], A. M. Lunev[a], V. E. Goncharenko[a, b], I. V. Taidakov[b], V. D. Dolzhenko[a], and Yu. A. Belousov[a, b]

[a] *Moscow State University, Moscow, Russia*

[b] *Lebedev Physical Institute, Russian Academy of Sciences, Moscow, Russia*

**e-mail: mariia.lavrova@chemistry.msu.ru*

Received October 11, 2021; revised November 19, 2021; accepted November 22, 2021

Abstract—New complex $[RuL(Dmdcbp)_2]PF_6$ (**I**) is synthesized by the consecutive reactions of $[Ru\text{-}p\text{-cymene}]_2Cl_4$ with 3,3',5,5'-tetramethyl-1,1'-biphenyl-4,4'-bipyrazole (L) and 4,4'-dicarboxy-2,2'-bipyridine in a methanol–chloroform medium. The composition of complex **I** is confirmed by NMR and elemental analysis, and the optical and luminescence properties of the complex are studied. Ligand L is characterized for the first time by X-ray diffraction (CIF file CCDC no. 2118676). Quantum chemical calculations in terms of the density functional theory are performed for the interpretation of the absorption and emission spectra. Complex **I** is promising for using as a photosensitizer.

Keywords: cyclometallation, ruthenium, Grätzel cell, bipyrazole

DOI: 10.1134/S1070328422060033

INTRODUCTION

Cyclometallated complexes of ruthenium(II) find use as anticancer drugs [1], materials for the photocatalytic reduction of CO_2 [2] and reduction [3] and oxidation [4] of water, and as dyes [5, 6] in dye-sensitized solar cells (DSSC, Grätzel cells).

The complexes for DSSC should contain an "anchor" ligand with acidic groups capable of covalently binding with the surface of titanium dioxide used in photoanodes of Grätzel cells and a "donor" ligand responsible for efficient solar light absorption [5, 6]. The ruthenium(II) thiocyanate complexes are the most studied compounds for DSSC [7]. They contain monodentate ligands leading to the lability of the complexes. In order to enhance the thermodynamic and kinetic lability of the complexes, it was proposed to introduce a bidentate cyclometallated ligand instead of monodentate ligands, which results in the formation of a metal–carbon covalent bond [8]. However, when the complexes with the cyclometallated fragment are used, the efficiency of operation of solar cells decreases compared to the cells based on the thiocyanate complexes.

We have previously studied the ruthenium(II) complexes based on 2-arylbenzimidazoles. The influence of the substituent nature on the photophysical and electrochemical properties of the complexes and on the operation efficiency in the cell was studied using the modification of the aryl fragment by various donor and acceptor substituents [9].

Phenylpyrazole ligands resemble benzimidazole ligands, but they are poorly studied [10–19]. The cyclometallated ruthenium complexes based on the 1-phenyl- and 3-phenylpyrazole derivatives were studied as anticancer drugs [13, 16, 17]; catalysts of C–C alkylation [10], cyclotrimerization [14], and reduction of ketones [12]; and photocatalysts of formic acid reduction [11].

1-Phenylpyrazoles are synthesized in high yields by the condensation of β-diketones with phenylhydrazine [20, 21]. The substituents can be varied by the introduction of a substituent into both the starting diketone [21, 22] and starting hydrazine [23]. In spite of synthetic availability [24], only unsubstituted bipyrazoles are well studied among bipyrazole ligands, whereas no complexes for *N*-phenyl-substituted bipyrazoles were obtained within more than 40 years since the publication of the synthesis procedure of the ligand [25].

Ligand 3,3',5,5'-tetramethyl-1,1'-biphenyl-4,4'-bipyrazole (L) is potentially capable of forming both mononuclear and binuclear complexes due to two coordination sites. Mononuclear complexes with this ligand should efficiently absorb solar radiation owing to the presence of many electron-donor groups. The mononuclear metal complexes have such drawbacks as

the possibility of the backward electron transfer from the conductivity band of TiO_2 and localization of the electron transfer and reduction processes.

The use of the binuclear complexes in DSSC allows one to provide the spatial separation of these processes to diminish undesirable transitions [25]. Electron transfer is possible in the binuclear complexes, which occurs under the action of the long-wavelength light with high molar absorption coefficients. This process would compete with the backward transfer thus decreasing its influence. In addition, the reduction would occur on the metal atom arranged at a longer distance from the TiO_2 surface, which prevents charge recombination [25].

The purpose of the present work is to synthesize the cyclometallated ruthenium(II) complex based on ligands L and Dmdcbp and to study its photophysical properties.

EXPERIMENTAL

The following commercially available reagents and solvents were used: $[Ru(p\text{-cymene})Cl_2]_2$, I_2 (reagent grade), KPF_6 (reagent grade), NaOH (special purity grade), acetylacetone, phenylhydrazine, and dimethyl ether of 4,4'-dicarboxy-2,2'-bipyridine (Dmdcbp).

Electronic absorption spectra were recorded in CH_3CN on an SF-2000 instrument in quartz 1-cm cells in a range of 400–900 nm. Photoluminescence spectra (PL) of solutions were measured on a Shimazu RF-1501 luminescence spectrometer. The measurements were carried out in quartz cells 1 cm in diameter at room temperature. NMR spectra were recorded at 25°C on a Bruker Avance 400 instrument, and chemical shifts are presented in ppm relative to signals of the solvent. High-resolution mass spectra (HRMS) were detected on a Bruker maXis Q-TOF instrument (Bruker Daltonik GmbH, Bremen, Germany).

Synthesis of sodium acetylacetonate (NaAcac). Sodium hydroxide (3.7 g) was dissolved in water (5 mL), and ethanol (18 mL) was added. The resulting solution was added (with a rate of 1 mL/min) to acetonitrile (9.16 g) with stirring in a conic 100-mL flask. The formed yellowish precipitate was cooled, filtered under reduced pressure on a glass filter, and washed with a minor amount of ice-cold methanol. The yield of $Na(Acac)\cdot 2H_2O$ was 11.67 g (81%).

Synthesis of 3,4-diacetylhexane-2,5-dione [26]. A solution of iodine (9.14 g) in dimethylformamide (DMF) (40 mL) was added (with a rate of 3 mL/min) to a solution of $Na(Acac)\cdot 2H_2O$ (11.67 g) in DMF (58 mL) with vigorous stirring. The resulting red-brown solution was poured into ice-cold water (400 mL), the mixture was stirred for 15 min, and the formed white precipitate was filtered off on a glass porous filter and washed with water. The yield was 4.66 g (65%).

^{1}H NMR (400 MHz; $CDCl_3$; δ, ppm): 2.01 (s, 12 H). ^{13}C NMR (400 MHz; $CDCl_3$; δ, ppm): 23 (s), 108 (s), 192 (s).

Synthesis of 3,3',5,5'-tetramethyl-1,1'-biphenyl-4,4'-bipyrazole (L) [27]. A solution of phenylhydrazine (1.26 g) (or 1.15 mL for ρ = 1.01 g/mL) and diacetylacetone (1.15 g) in ethanol (11.5 mL) was refluxed for 24 h. The solution turned transparent and orange on reflux. The solution was evaporated to dryness, the dry residue was recrystallized from cyclohexane, and colorless crystals precipitated on cooling. The obtained precipitate was washed with cyclohexane (1 mL) and dried. The yield was 1.85 g (93%).

^{1}H NMR (400 MHz; $CDCl_3$; δ, ppm): 2.21 (s, 6 H), 2.21 (s, 6 H), 7.33–7.39 (m, 2 H), 7.45–7.55 (m, 8 H). ^{13}C NMR (400 MHz; $CDCl_3$; δ, ppm): 11 (s), 12 (s), 112 (s), 124 (s), 127 (s), 129 (s), 137 (s), 139 (s), 148 (s).

Synthesis of $[RuL(CH_3CN)_4]PF_6$. A flask with a tightly screwed top was filled with L (0.165 g, 0.48 mmol), NaOH (0.0094 g, 0.24 mmol), and KPF_6 (0.089 g, 0.48 mmol). The mixture in the flask was dissolved in acetonitrile (5 mL) preliminarily saturated with argon, and argon was passed through the mixture on heating. Compound $[Ru(p\text{-cymene})Cl_2]_2$ (0.0735 g, 0.12 mmol) was dissolved in dichloromethane (2 mL), and the resulting solution was added to the reaction mixture. A dark red solution was formed. The tube was maintained at 45°C for 72 h. The obtained dark brown solution was evaporated to dryness, and the residue was dissolved in methylene and purified by column chromatography (silica gel, eluent CH_2Cl_2–CH_3CN (10 : 1)). A yellow fraction was collected. The precipitate was salted out with hexane and evaporated to dryness. The yield was 0.15 g (83% based on $[Ru(p\text{-cymene})_2Cl_2]_2$).

Synthesis of $[RuL(Dmdcbp)_2]PF_6$ (I). Compounds $[RuL(CH_3CN)_4]PF_6$ (0.15 g, 0.2 mmol) and Dmdcbp (0.109 g 0.4 mmol) in a mixture of MeOH (5 mL) and CH_2Cl_2 (5 mL) were refluxed under argon in the dark for 24 h. The formed black solution was evaporated to dryness. The obtained substance was purified by column chromatography (silica gel, eluent CH_2Cl_2–CH_3CN (85 : 1)). Elution was conducted slowly for good separation. The colored fraction was collected. Then recrystallization was carried out: the substance was dissolved in a methylene–hexane (3 : 2 vol/vol) mixture (10 mL), and the resulting mixture was left in a refrigerator for 24 h. Black crystals precipitated from the solution were separated on a glass porous filter, washed with hexane, and dried in vacuo. The yield was 0.206 g (91%).

^{1}H NMR (400 MHz; $CDCl_3$; δ, ppm): 1.96 (s, 3 H), 2.18 (m, 6 H), 2.65 (s, 3 H), 4.03 (m, 12 H), 6.80 (t, J = 6.85 Hz, 1 H), 7.00 (br.s, 1 H), 7.37–7.50 (m, 5 H), 7.56–7.60 (m, 1 H), 7.71–7.75 (m, 1 H), 7.75–

Table 1. Crystallographic data and experimental and structure refinement parameters for compound L

Parameter	Structure
Empirical formula	$C_{22}H_{22}N_4$
FW	342.43
Recording temperature, K	293(2)
Crystal system	Monoclinic
Space group	$P2_1$
a, Å	10.258(2)
b, Å	7.8910(16)
c, Å	11.334(2)
β, deg	99.02(3)
V, Å^3	906.1(3)
Z	2
ρ_{calc}, g/cm^3	1.255
$\mu(MoK_\alpha)$, mm^{-1}	0.076
F(000)	364
θ_{min}–θ_{max}, deg	2.491–29.999
Total number of reflections	6872
Number of independent reflections (R_{int})	5087 (0.0253)
Number of reflections with $I > 2\sigma(I)$	4568
Number of parameters	240
R factors (for reflections with $I > 2\sigma(I)$)	$R_1 = 0.0500$, $wR_2 = 0.1118$
R factors (for all reflections)	$R_1 = 0.0580$, $wR_2 = 0.1151$
GOOF	1.058
$\Delta\rho_{max}/\Delta\rho_{min}$, e/Å^3	0.342/–0.336

7.91 (m, 3 H), 7.95–7.99 (m, 1 H), 8.03–8.10 (m, 1 H), 8.26 (d, J = 7.89 Hz, 1 H), 8.28–8.38 (m, 1 H), 8.78 (t, J = 10.12 Hz, 2 H), 8.89–8.97 (m, 2 H). HRMS, *m/z*: found 987.2393, calculated for $C_{50}H_{45}N_8O_8Ru^+$ 987.2412, the isotope peak distribution coincides with the calculated one.

X-ray diffraction (XRD) of a single crystal of compound L was carried out on a Bruker D8 Quest diffractometer with a Photon III detector (MoK_α radiation, λ = 0.71073 Å, ω scan mode) at 293(2) K. The structure was solved by direct methods and refined by full-matrix least squares for F^2 using the SHELXTL and Olex2 program packages [28–30]. Hydrogen atoms were placed in the calculated positions and refined using the riding model. Ligand L crystallizes in the chiral space group, but the absolute configuration of the structure was not determined because of anomalously weak X-ray scattering caused by the absence of heavy atoms in the structure. The crystallographic data and experimental and structure refinement parameters are presented in Table 1.

The atomic coordinates, bond lengths, bond angles, and thermal shift parameters were deposited with the Cambridge Crystallographic Data Centre (CIF file CCDC no. 2118676; deposit@ ccdc.cam.ac.uk or http://www.ccdc.cam.ac.uk).

Quantum chemical calculations were performed in the FireFly program package [31] using the B3LYP functional. The Stuttgart RSC 1997 basis set with the pseudopotential was used for the ruthenium atom. The 6-311G(d,p) basis set was used for other atoms (C, N, H, and O). This combination of basis sets and

functional gives a good correlation with experiment [32]. The initial coordinates of the molecule of ligand L are based on its crystal structure, and the arrangement of dimethyl ether of dicarboxybipyridine molecules were taken from the structure of the complex with another C^N-donor ligand [9]. The geometry of the triplet state was optimized for the estimation of the emission wavion using the time-dependent density functional theory (TD-DFT) to obtain excitation energies for modeling the absorption spectrum of the complex. Vibration frequencies were calculated for optimum geometries, and no imaginary frequencies were observed (low imaginary frequencies to -10 cm^{-1} induced by inaccuracies in the integration network were ignored). Visualization was performed using the ChemCraft v. 1.8 software.

RESULTS AND DISCUSSION

The crystal structure of the ligand is shown in Fig. 1. The crystals were prepared by cooling a solution of the ligand in hot dimethyl sulfoxide (DMSO), but they contain no solvent molecules. Remarkably, in the formed structure all aromatic fragments lie in different planes and, hence, they are not conjugated to each other. The torsion angles between the planes of the pyrazole fragment and phenyl substituent are as follows: N(1)–N(2)–C(6)–C(5) 128.5(2)° and N(4)–N(3)–C(17)–C(18) 142.1(2)°. The C(10)–C(9)–C(12)–C(15) angles between the pyrazole fragments are 48.8(4)°. No π-stacking interactions are observed for the packing of the molecules in the cell.

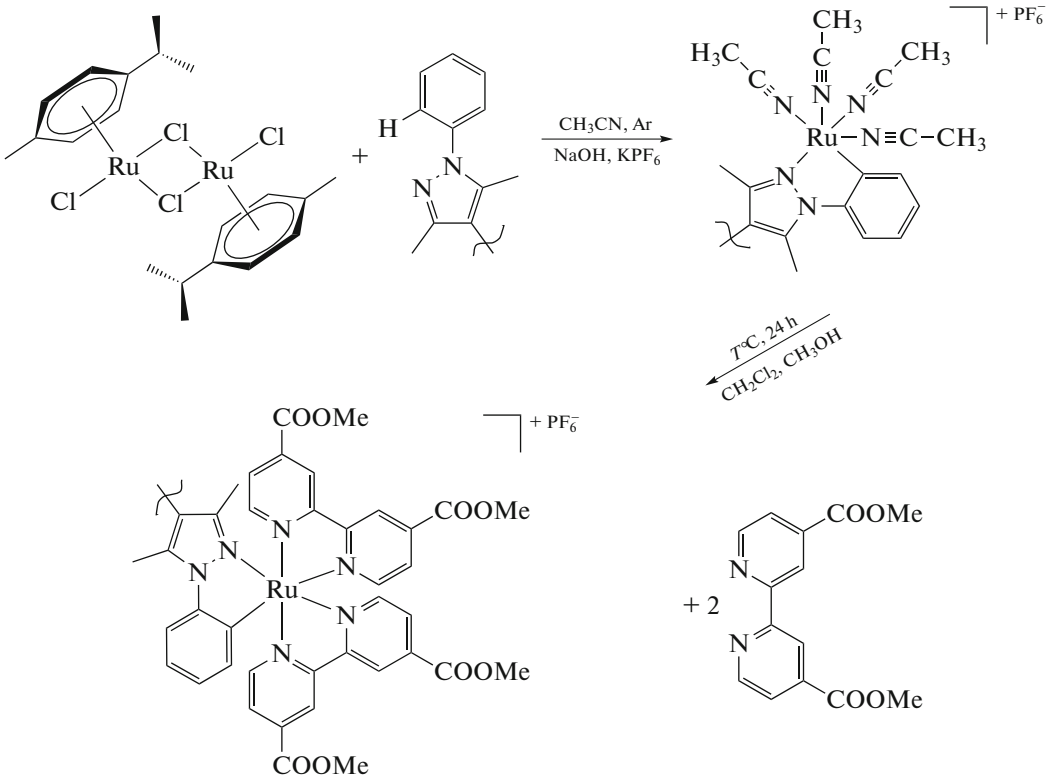

Scheme 1.

Complex $[RuL(Dmdcbp)_2]PF_6$ (**I**) is synthesized in two stages (Scheme 1). Cyclometallation was carried out at the first stage, and dimethyl 2,2'-bipyridine-4,4'-dicarboxylate (Dmdcbp) was introduced at the second stage. The first stage affords a product readily oxidized in air and, therefore, the product was used in the second stage without intermediate characterization. The literature data [5] indicate that a complex with four acetonitrile molecules is formed and, hence, we assume a similar composition.

Complex **I** synthesized at the second stage is mononuclear; i.e., the bipyrazole ligand coordinates to the metal by only one half, which is confirmed by the number of ratio of signals in the NMR spectrum. The signals in a range of 6.5–7.0 ppm indicate the ruthenium–carbon covalent bond (Fig. 2). The most intense signal in the mass spectrum corresponds to the $[RuL(Dmdcbp)_2]^+$ cation, which is confirmed by the isotope distribution data (Fig. 3).

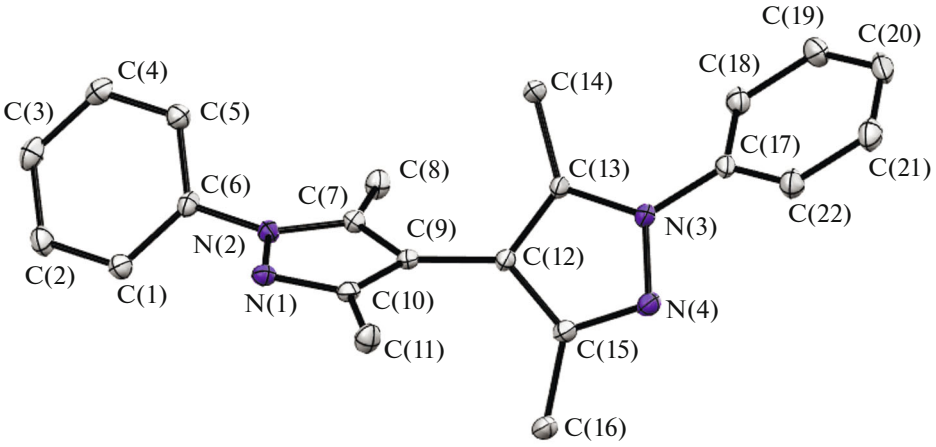

Fig. 1. Molecular structure of L. Hydrogen atoms are omitted, and thermal ellipsoids are shown with 50% probability.

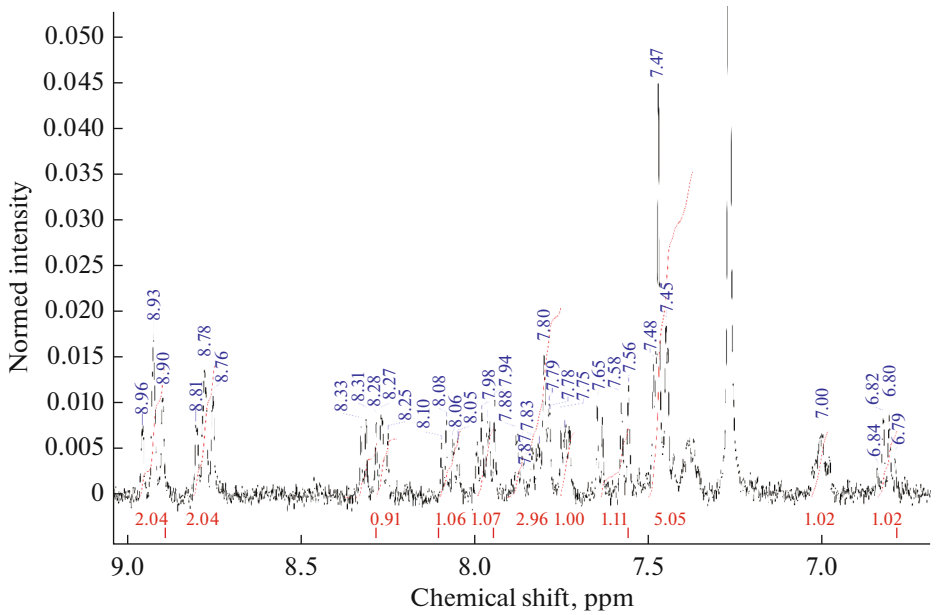

Fig. 2. Aromatic fragment of the NMR spectrum of complex **I**.

The molar absorption coefficients were determined for complex **I**. The resulting spectrum was expanded to the Gaussian components using least squares (Fig. 4). According to the data of TDDFT calculations, the electron transitions in the visible range correspond to metal-to-ligand charge-transfer (MLCT) transitions.

The complex efficiently absorbs in the visible range: the long-wavelength band with the absorption maximum at 735 nm is characterized by a fairly high extinction ($\varepsilon = 1800$ L mol^{-1} cm^{-1}), which exceeds the value observed in this range for classical dyes N3 and black dye [5].

The PL spectra of complex **I** were measured for a dilute solution in acetonitrile (Fig. 5). The energy of the excitation state was estimated from the position of the emission band as equal to 11 500 cm^{-1}.

The electronic structure of the complex was studied using the DFT method. The main contribution to the highest occupied molecular orbitals (HOMO) is made by the *d*-orbitals of the metal and π-orbitals of the C^N-donor ligand (Table 2). In the complex considered, symmetric ligand L capable of performing the bridging function is coordinated only via one coordination site. Interestingly, orbital H is localized on ligand L, and orbitals H-1, H-2, and H-3 are localized

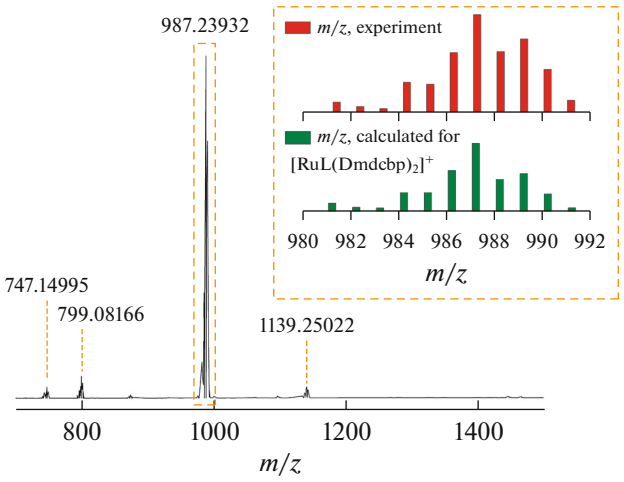

Fig. 3. HRMS spectrum of complex **I**. Inset: magnified fragment corresponding to the peak at $m/z = 987.23932$ and calculated data for cation $[RuL(Dmdcbp)_2]^+$.

on the metal (Fig. 6). The lowest occupied molecular orbitals (LUMO) are localized on the dicarboxybipyridine ligands involving the *d*-orbitals of the metal.

The characteristics of 25 excited states were calculated for the TDDFT modeling of the absorption spectra. The positions, intensities of the transitions, and envelope at the fixed linewidth of the absorption bands of particular transitions are shown in Fig. 3 (inset).

The emission wavelength ($\lambda_{0\text{-}0}$) was estimated from the difference in energies of the triplet and singlet states for the optimized geometry in the triplet state (ΔSCF). The calculated value (930 nm) is shifted to the long-wavelength range relative to experiment, which is consistent with published data [33]. The HOMO of the triplet state is localized on the anchor ligands containing the carboxyl groups (Fig. 7).

Thus, complex $[RuL(Dmdcbp)_2]PF_6$ satisfies the main requirements [5] imposed on photosensitizers for DSSC: high absorption in the visible range, HOMO orbitals localized on donor ligand L and metal, and LUMO orbitals localized on the acceptor anchor ligand Dmdcbp.

ACKNOWLEDGMENTS

This work was carried out using the equipment purchased at the expense of facilities of the development program of the Moscow State University.

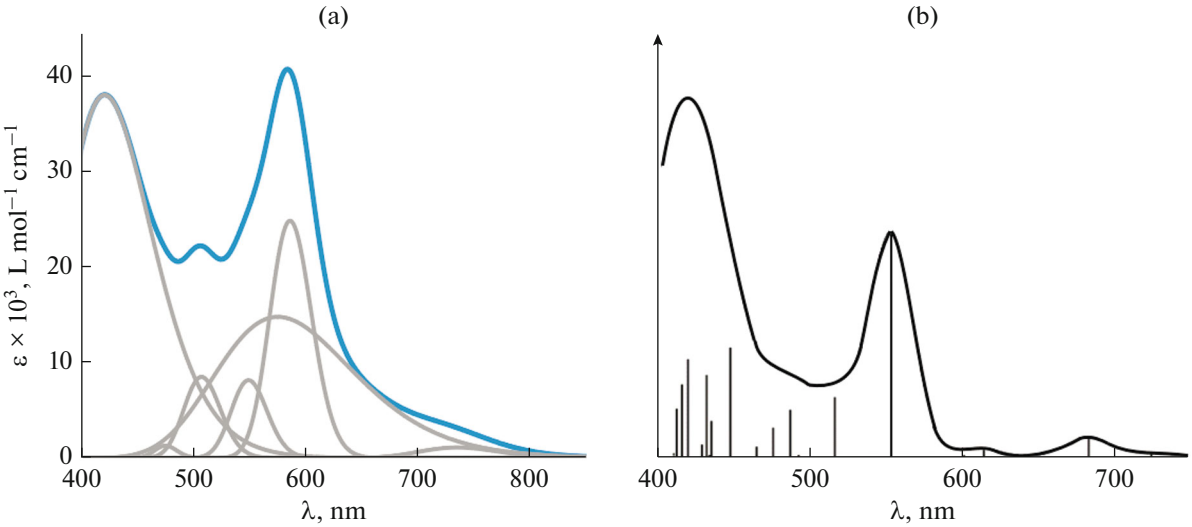

Fig. 4. (a) Absorption spectrum of complex **I** in acetonitrile with expansion to the Gaussian components and (b) TDDFT calculation results of vertical transitions.

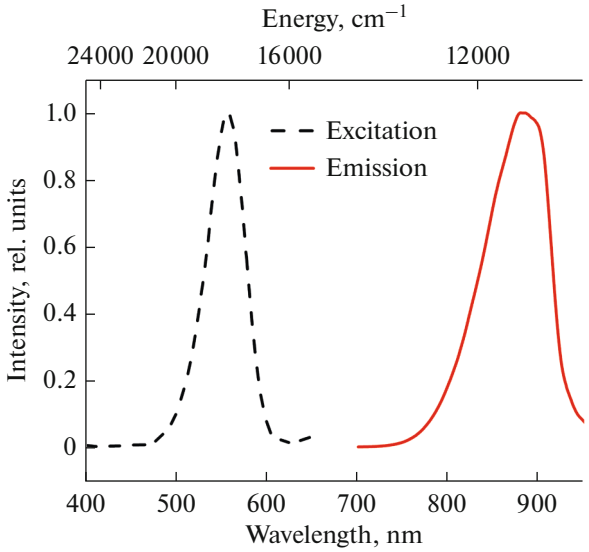

Fig. 5. Excitation (λ_{exc} = 890 nm) and emission (λ_{em} = 550 nm) spectra of a solution of $[RuL(Dmdcbp)_2]PF_6$ in CH_3CN.

Table 2. Selected calculated spectral characteristics of the $[RuL(Dmdcbp)_2]^+$ complex: excited states, wavelengths (λ, nm), oscillator forces, and assignment of electron transitions with contributions of the corresponding configurations

State	λ, nm	Oscillator force	Main contributions from MO transitions			
S^2	725	0.012	HOMO	→	LUMO + 1	73.7%
S^5	553	0.13	HOMO-3	→	LUMO	13.4%
			HOMO-2	→	LUMO	22.9%
			HOMO-2	→	LUMO + 1	15.5%
			HOMO-1	→	LUMO	32.1%
S^6	516	0.035	HOMO-2	→	LUMO + 1	36.4%
			HOMO-1	→	LUMO	11.3%
			HOMO-1	→	LUMO + 1	13.0%
			HOMO	→	LUMO + 3	12.4%
S^8	487	0.028	HOMO-3	→	LUMO	35.6%
			HOMO	→	LUMO + 2	39.1%
S^{12}	447	0.064	HOMO-3	→	LUMO + 1	33.5%
			HOMO	→	LUMO + 3	13.1%
			HOMO	→	LUMO + 4	22.3%

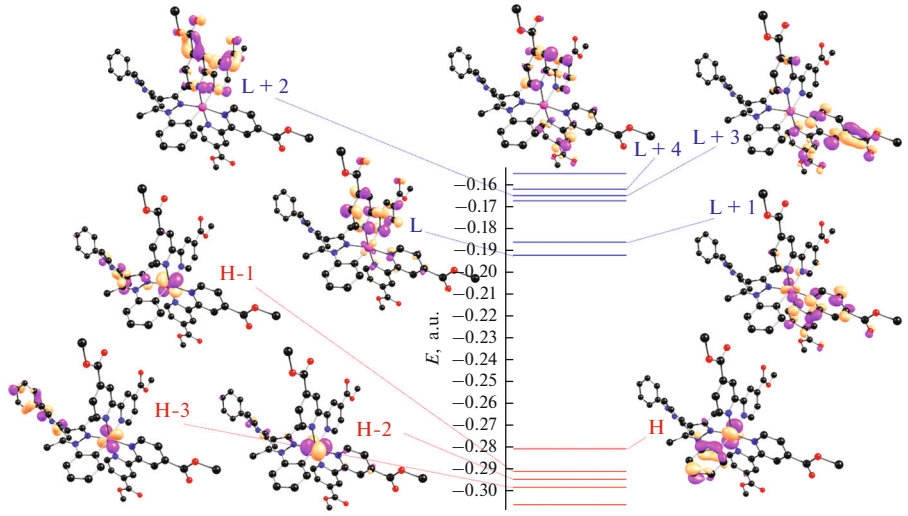

Fig. 6. Scheme of the molecular orbitals of the $[RuL(Dmdcbp)_2]^+$ complex and frontier orbitals.

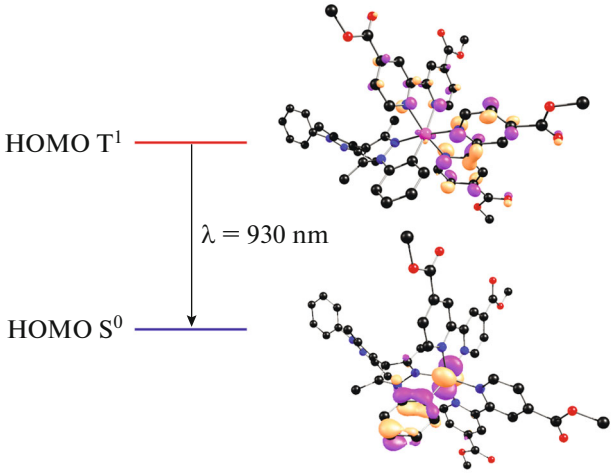

Fig. 7. HOMO of the singlet and lowest triplet states of the $[RuL(Dmdcbp)_2]^+$ complex by the DFT calculation.

FUNDING

This work was supported by the Russian Foundation for Basic Research, project no. 20-33-90285.

CONFLICT OF INTEREST

The authors declare that they have no conflicts of interest.

OPEN ACCESS

REFERENCES

1. Huang, H., Zhang, P., Chen, H., et al., *Chem.-Eur. J.*, 2015, vol. 21, p. 715.
2. Ono, T., Qu, S., Gimbert-Surinach, C., et al., *ACS Catal.*, 2017, vol. 7, p. 5932.
3. Yuan, Y.J., Yu, Z.T., and Chen, D.Q., *Chem. Soc. Rev.*, 2017, vol. 46, p. 603.
4. Tseng, H., Zong, R., Muckerman, J.T., and Thummel, R., *Inorg. Chem.*, 2008, vol. 47, p. 11763.
5. Aghazada, S. and Nazeeruddin, M.K., *Inorganics*, 2018, vol. 6, p. 52.
6. Mauri, L., Colombo, A., Dragonetti, C., et al., *Molecules*, 2021, vol. 26, p. 7638.
7. Zakeeruddin, S., Nazeeruddin, M., Humphry-Baker, R., and Grätzel, M., *Inorg. Chim. Acta*, 1999, vol. 296, p. 250.
8. Bomben, P.G., *Cycloruthenated Chromophores for the Dye-Sensitized Solar Cells*, Calgary, 2012.
9. Lavrova, M.A., Mishurinskiy, S.A., Smirnov, D.E., et al., *Dalton Trans.*, 2020, vol. 49, p. 16935.
10. Korvorapun, K., Moselage, M., Struwe, J., et al., *Angew. Chem., Int. Ed. Engl.*, 2020, vol. 59, p. 18795.
11. Nakahara, Y., Toda, T., Matsunami, A., et al., *Chem. Asian J.*, 2018, vol. 13, p. 73.
12. Toda, T., Saitoh, K., Yoshinari, A., et al., *Organometallics*, 2017, vol. 36, p. 1188.

13. Novohradsky, V., Yellol, J., Stuchlikova, O., et al., *Chem.-Eur. J.*, 2017, vol. 23, p. 15294.
14. Grigg, R., Kilner, C., Senthilnanthanan, M., et al., *Arkivoc*, 2007, vol. 2007, p. 145.
15. Alharis, R.A., McMullin, C.L., Davies, D.L., et al., *Faraday Discuss*, 2019, vol. 220, p. 386.
16. Ballester, F.J., Ortega, E., Porto, V., et al., *Chem. Commun.*, 2019, vol. 55, p. 1140.
17. Kamatchi, T.S., Kalaivani, P., Fronczek, F.R., et al., *RSC Adv.*, 2016, vol. 6, p. 46531.
18. Boutadla, Y., Davies, D.L., Jones, R., and Singh, K., *Chem.-Eur. J.*, 2011, vol. 17, p. 3438.
19. Toda, T., Suzuki, S., and Kuwata, S., *Chem. Commun.*, 2019, vol. 55, p. 1028.
20. Reddy, C.S., Kumar, G.R., Devi, M.V., and Nagaraj, A., *Acta Chim. Slov.*, 2011, vol. 58, p. 576.
21. Svistunova, I.V., Shapkin, N.P., Nikolaeva, O.V., and Apanasenko, O.A., *Russ. J. Gen. Chem.*, 2011, vol. 81, p. 756.
22. Chambers, D., Denny, W.A., Buckleton, J.S., and Clark, G.R., *Org. Chem.*, 1985, vol. 50, p. 4736.
23. Texier-Boullet, F., Klein, B., and Hamelim, J., *Synthesis*, 1986, vol. 1986, p. 409.
24. Mosby, W.L., *J. Chem. Soc.*, 1957, p. 3997.
25. Anon, I., *Bulletin de la Societe Chimique de France*, 1975, p. 1371.
26. Ponomarova, V.V., Komarchuk, V.V., Boldog, I., et al., *CrystEngComm*, 2013, vol. 15, p. 8280.
27. Imai, Y., Nakajima, T., and Ueda, M., *J. Polym. Sci.*, 1981, vol. 19, p. 1421.
28. Sheldrick, G.M., *Acta Crystallogr., Sect. C: Struct. Chem.*, 2015, vol. 71, p. 3.
29. Sheldrick, G.M., *Acta Crystallogr., Sect. A: Found. Adv.*, 2015, vol. 71, p. 3.
30. Dolomanov, O.V., Bourhis, L.J., Gildea, R.J., et al., *J. Appl. Crystallogr.*, 2009, vol. 42, p. 339.
31. Granovsky, A.A., Firefly version 8. http://classic.chem.msu.su/gran/firefly/index.html.
32. Derrat, H.S., Robertson, C.C., Meijer, A.J.H.M., and Thomas, J.A., *Dalton Trans.*, 2018, vol. 47, p. 12300.
33. Soupart, A., Dixon, I.M., Alary, F., and Heully, J.L., *Theor. Chem. Acc.*, 2018, p. 137.

Translated by E. Yablonskaya